Lasers in Manufacturing Conference 2015

Some optimization strategies for tool path generation in 3D laser metal deposition

J.N. Montero, A. Rodríguez, J.M. Amado, M.J. Tobar*, A. Yáñez

Universidade da Coruña, Dpto. Ingeniería Industrial II, Ferrol, E-115403, Spain

Abstract

Laser direct metal deposition has proven to be successful in the manufacturing of 3D parts. In this process, the required geometry is built up layer by layer on overlapping laser clad beads. However, some problems are often encountered regarding surface finish and dimensional accuracy. These are mainly caused by heat accumulation effects during the process (resulting in changes in material temperature and powder catchment efficiency) and/or inadequate tool path trajectories and scanning parameters. All these factors lead to defects in the manufactured 3D part, particularly when bulk solid structures (as opposed to hollow) are involved in the process.
In this work we test and discuss the effect of different tool path strategies in dealing with the above issues. Results will be presented on the laser 3D manufacturing of stainless steel parts. A monitoring device (online CMOS camera) will be used to supervise and get and better understanding of the deposition process under the different approaches.

Keywords: Additive Manufacturing

1. Introduction

In recent years Laser metal deposition technologies (LMD) have reached great popularity as a solution for manufacturing of rapid prototyping parts and 3D printing. Despite big improvements in this field a lot of challenges have yet to be overcome. Some of the limitations of LMD when compared to other 3D manufacturing technologies as Electron Beam Manufacturing (EBM) or Selective Laser Melting (SLM) are poor surface finish and dimensional accuracy. However LMD presents a series of advantages as higher deposition rates, bigger working areas and less porosity.

Many studies have been carried out in order to diminish these problems. Close loop control techniques have been researched employing a wide set of monitoring systems and control strategies, Tuomas Purtonen et al, 2014. Among the monitoring systems used optical imaging systems as CCD and CMOS cameras stand out. Parametric studies have been performed to improve the accuracy and the surface finish of the process, Myriam Gharbi et al, 2013; G.A. Ravi et al, 2013. Also it is worth to mention other studies that have shown the importance of the path planning effect in the surface finish of the parts, Donghong Ding et al, 2015 and the microstructure, Abdalla R. Nassar, 2015.

In the present work, based on some of these ideas, a study of the effects of tool path plans in the manufacturing of bulk stainless steel blocks is proposed. An analysis of the deposition process is carried out by means of an online monitoring system which consists of a CMOS camera synchronized with the positioning system of the LMD machine, allowing the retrieval of the part cross section geometry in real time. The data obtained can be used for developing different kind of path-plan optimization strategies. This fact is proven by the implementation of an iterative method for improving dimensional accuracy in the laser metal deposition process.

2. Experimental setup

The laser metal deposition system is composed of a continuous wave diode pumped Nd:YAG laser (Rofin DY022) with a maximum power of 2200 W. Laser is sent through a fiber to the YC50 Precitec claddind head installed in a ABB IRB2400 six axis robot arm. Powder feeding is made with a Sulzer-Metco Twin 10C unit. A custom application controls and monitors all the steps of the process. Programming commands are transmitted via ftp and loaded into the ABB motion controller. Once loaded, the controller takes upon the movement of the robot according to the programmed speed and trajectory. It also sends the required voltage signals for switching on the laser and the powder feeder and sets the required laser power and powder flow levels during the process. Return monitoring signals from laser metal deposition head and powder feeder are directly transmitted to the PC application for process supervision.

The powder used is METCO 41C austenitic stainless steel. Cladding is performed on 10 mm thick probes of A316L grade stainless steel. Laser beam is defocused to a diameter of 2 mm on the working surface.

A CMOS camera connected to the PC by a frame grabber is used to monitor the process. The camera lens is a 130 mm zoom lens. An optical filter is placed in front of the camera lens in order to suppress the laser radiation (1024 nm).

The camera is positioned in front of the clad, such as the forming clad moves along the optical axis and towards the camera, so the front view of the melt pool is captured by the imaging device.

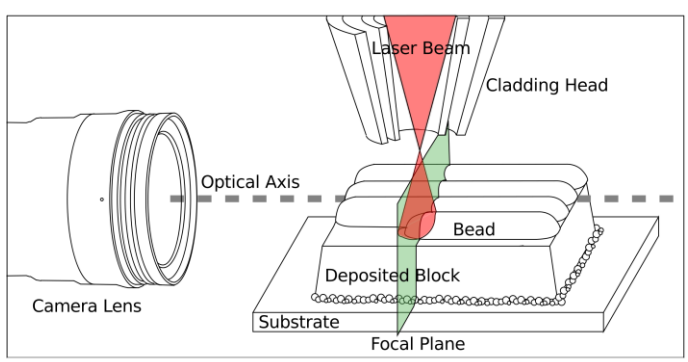

Fig. 1. Experimental set-up diagram showing the camera lens and its focal plane position relative to the part and LMD head.

The lens is focused at its maximum magnification and the focal plane is positioned 20 mm from the laser activation point. Depth of field obtained is around 2 mm. A timer triggered by a laser signal is used to start the image acquisition when the laser spot reaches the focal plane of the camera. Camera exposure is adjusted to make segmentation easier, looking for a high contrast between the melt pool and the remainder image. The images are obtained at regular intervals during the time the LMD head travels through the 2mm of focal plane. Acquisition time never surpass 10 us per image.

The images from the camera are sent to a computer and processed in real time by a custom program developed by the authors.

Five tests samples are built with the process parameters shown in the Table. 1. Each sample is built stacking 14 layers of 5 overlapped tracks. The build order is changed in every sample as shown in Fig.6. During the process, images are acquired in order to reconstruct and analyze the geometry of the deposits in real time.

Table 1. Process parameters

Process parameters	Value
Laser	CW Nd-YAG
Laser power	1000 W
Spot diameter	2 mm
Scanning speed	20 mm/s
Powder feed rate	160 mg/s
Overlapping ratio	0.33
Δz between layers	0.4 mm

3. Results

3.1. Image segmentation

The bead cross section is determined real-time from the images of the melt pool using a custom software.

For each bead of the sample a set of images is acquired (between 12 and 20). In those images the pixels belonging to the melt material present intensity levels close to the saturation level of the sensor, allowing the use of a threshold method to carry out the segmentation.

Fig. 2. (a) gray scale image of the melt pool; (b) segmentation of the melt pool

The segmentation is not straightforward and some problems arise due to the presence of powder particles with intensity levels close to those of the melt clad and solid particles between the camera and the melt pool occluding the image.

As the particles are moving bodies they can be eliminated by averaging the intensity values of every pixel position along the set of images to obtain a single image, as shown in Fig.2.

The temperature of the beads is not constant during the process, which causes the image of each one to be taken at a different temperature. The intensity of the pixels in the gray level images is proportional to their temperature, therefore the threshold used for the segmentation should be different for each image, Sörn Ocyloka et al, 2014. Because the temperature of each clad is not known a priori, an average value of intensities is chosen for the threshold such as the bottom part of the melt pool agrees with the contour of the solid surface on which the clad is deposited for most of the images.

The resultant images are binarized with the given threshold and the contours of the clads are retrieved from the binary image using the algorithm from Suzuki, S. and Abe, K., 1985.

The Fig. 3 shows the obtained contours superimposed on a cross-section of the coating block. It can be seen that the contours fit the block accurately, except in its lateral walls where the size of the tracks is overestimated. The extra area corresponds to the melted material which slipped down the wall during the deposition, hence not becoming part of the final clad.

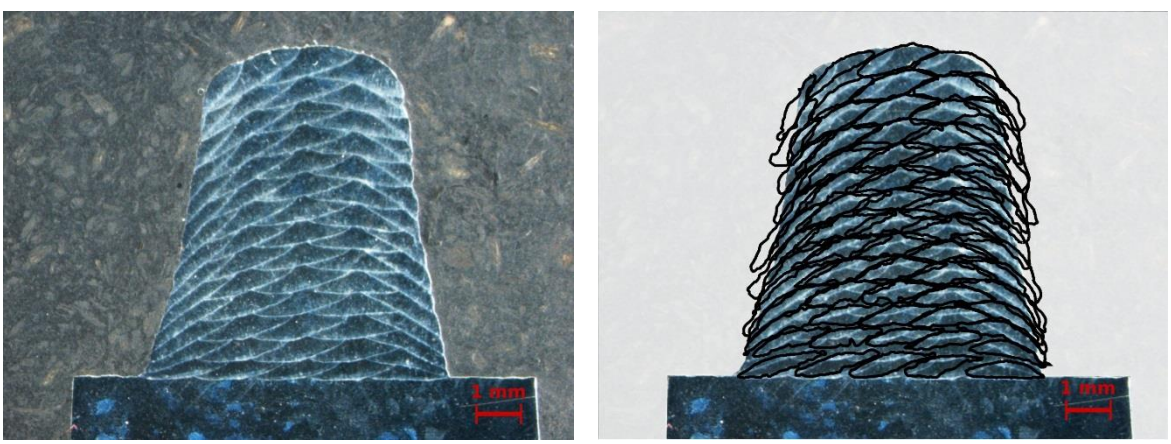

Fig. 3. (a) etched cross-section of a block showing bead frontiers; (b) bead contours over superimposed on the block cross section.

Several data can be retrieved from the contours of the clads, as height, width, overlapping ratio or powder efficiency (Fig. 4). In addition if the contours obtained by the camera and the ones appearing on the cross section of the block are compared, the dilution on each clad can be calculated, information that otherwise would be difficult to obtain.

For the tracks shown in Fig.4, the area surrounded by green lines consists on the material already presented in the block and remelted during the deposition. The blue contours represent the material deposited in this layer. The area surrounded by red contours corresponds to the part of the clad which is remelted during the subsequent deposition of other clads. The area filled with a crosshatch pattern represents the part of the clad which is not melted by the subsequent deposition of other clads.

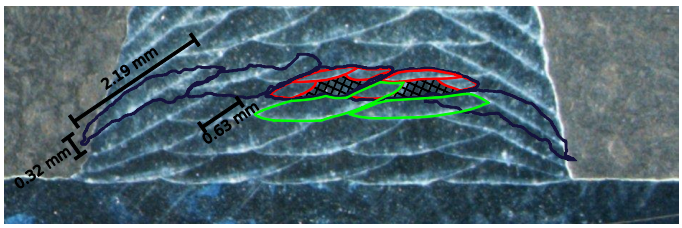

Fig. 4. Deposited layer diagram showing remelted areas.

The overlapping ratio, which quantifies the fraction of the clad that overlaps with its neighbours, can be calculated from the contours and therefore it is possible to compare the measure in the images with the ratio targeted in the experiment. The powder efficiency can be measured as well. The powder feed rate, the approximate density of the bulk material and the scanning velocity of the laser are known, which allows the calculation of the cross section area of a deposited clad for 100% efficiency. The ratio between this value and the area of the contour obtained by the segmentation gives an estimation of the powder efficiency of the process.

Finally, dilution can be estimated as the ratio between the areas surrounded by the blue and the green contours.

Data obtained from Fig 4 is presented in the Table 2 and data from the whole block is shown in Fig 5.

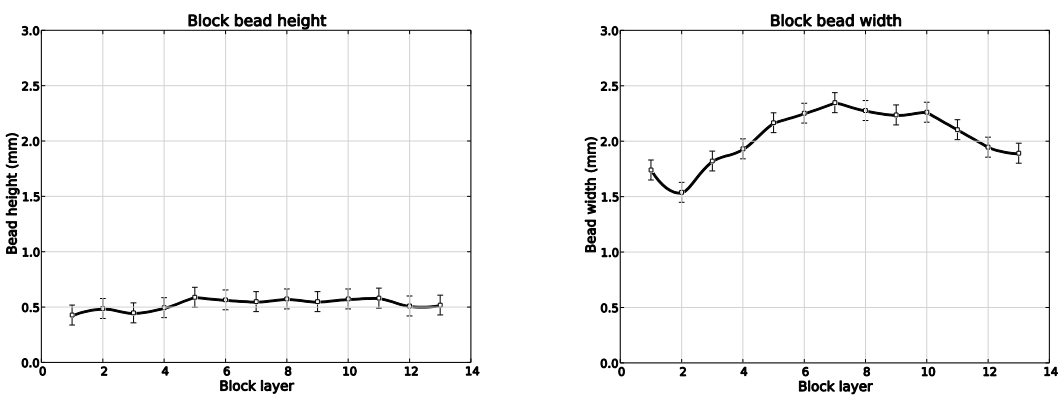

Fig. 5. Graphs of bead height and width measured by layer.

Table 2. Data from a bead of the Fig. 4.

Bead data	Value
Dilution	35 %
Efficiency	65 %
Overlapping angle	32º

3.2. Strategies

The complex physical phenomena involved in the laser metal deposition process makes very difficult to predict a priori the geometry of the beads which causes that the processing parameters need to be found empirically. The dimensional accuracy not only depends on the process parameters but also on the geometry of the part and the path planning used. When the process is executed without a close loop control, the geometric distortions accumulated from previous layers cannot be corrected, which causes deviations between the manufactured part and the original model. Also, it is difficult to guarantee that the process reaches a stationary state, leading to an overheating of the part or low efficiencies.

With the proposed method, feedback from the final geometry of the block is retrieved, allowing its study in real time or after the process. The images taken by the camera allow the chronological reconstruction of the deposition and they provide information that otherwise would not be possible to obtain even with destructive tests. Also, regions where errors were originated due to a bad deposition can be studied and the errors can be corrected if necessary.

The quality of the data obtained as well as the ability to analyze it during the process allows the implementation of new tool path planning optimization strategies. As they can be genetic algorithms, adaptive controls, neural networks and other techniques of optimization and test automation.

As an example, in this work, the improvement of the manufacturing of a stainless steel bulk part is shown. In order to achieve this improvement the difference between the experimental part section and the model section is measured. The bead deposition order is changed to minimize this difference leading to the usage of a series of path patterns.

The patterns tested are shown in Fig.6. The numbers inside the clads show the order in which the depositions are made.

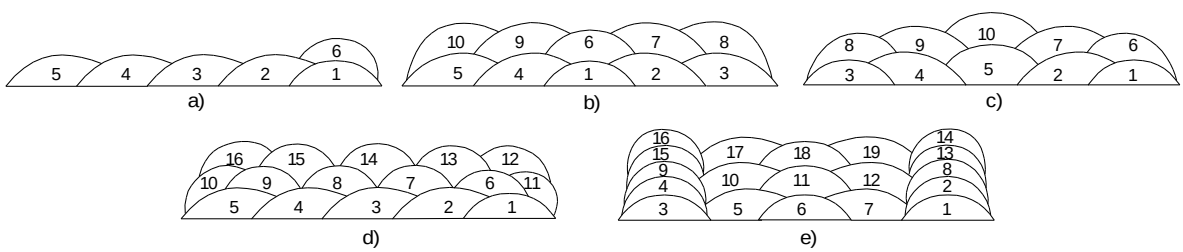

Fig. 6. Build path order diagrams.

In the first pattern of the Fig.6 each layer is made-up of parallel straight trajectories where each clad is deposited right after its immediate neighbour. Because the deposition of the block is not symmetrical, the geometry obtained in both lateral sides of the block will not be the same. As the height of the block grows, so does the angle of the surface on which the lateral clads are deposited which causes the loss of material due to the sliding of part of the molten zone on the wall down. Because of this fact the lateral walls of the block are not perfectly vertical, as shown in Fig.7a.

In the second one (of the Fig.6), the central clad of each layer is deposited first and then the adjacent clads are built, moving towards the sides of the block.

The third strategy of the Fig.6 represents the opposite strategy. The deposition begins with the clads of the sides and it ends with the clad of the center of the layer. The same pattern is repeated in every layer.

In the fourth strategy the first layer is deposited in the same way as in the first strategy, with the tracks following parallel straight trajectories where each clad is built after is neighbour. The difference with the first strategy is that in the second layer the position of the clads is displaced so they lay down in the center between

two adjacent clads of the layer below as shown in the d diagram of the Fig.6. This strategy tries to achieve a more uniform height along each layer.

In the fifth strategy shown in Fig.6, the construction of the lateral walls is made prior to the deposition of the interior clads. The pattern consist of two steps. In the first one, two beads are built at each border, one in top of the other with a 0.2 mm vertical offset. Then a layer is deposited between the side beads. The second step is done following the same order than the layer below, raising the LMD head 0.4 mm but only with one clad deposited on each outer border. This pattern is repeated until the targeted height is reached.

Building the walls this way prevents the clads of the side to slide down the wall, because the surface on which each clad is deposited is kept almost horizontal during the grow of the block.

In Fig.7 the contours of the blocks obtained by the techniques explained above are shown.

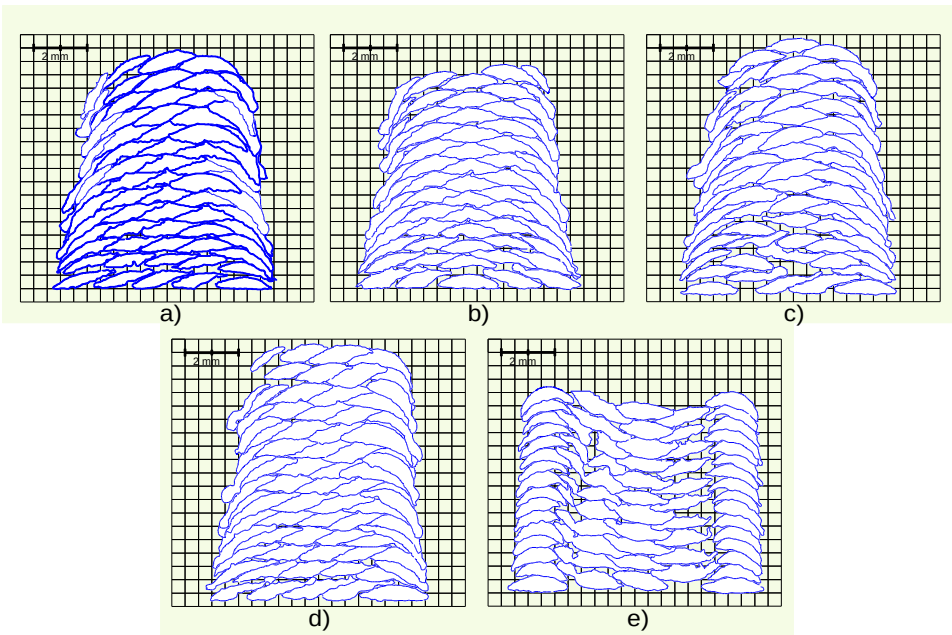

Fig. 7. Cross sections of the beads obtained by the online monitoring system showing the reconstructing of the blocks.

Similar results regarding the fitting of both model and experimental cross sections are found for the first four path plans tested. The best section fit is achieved with the fifth strategy, although problems with the overlapping angle of the internal layer are observed, producing voids inside the solid. An iterative adjustment is used to minimize this effect by changing the overlapping rate. The final obtained block presents a good agreement with the target section.

4. Conclusions

Different test samples have been built. Measures of height width, area and efficiency of each bead have been obtained as well as the contour of the whole section without using destructive tests. The online analysis of data has helped to optimize the building strategy of the parts to fit the target geometry.

The experimental setup presents a series of problems. The limited field of view of the camera does not let the acquisition of very large sections. Other problems are the difficult alignment of the optical system which may require an automatic positioning system.

Also, regarding the segmentation and analysis of the images taken some problems arise. Uncertainties finding the correct threshold are a main source of error and the presence of the feeding powder and other elements blocking the area of interest difficulties the analysis of the images. This can be improved by changes in the optical system.

For future work the geometrical data obtained could be used as input to a real time close loop control or as input to construct a model for the numerical analysis of the process.

References

Tuomas Purtonen, Anne Kalliosaari, Antti Salminen, 2014, Monitoring and adaptive control of laser processes, Physics Procedia 56, pp. 1218 – 1231.

Myriam Gharbi, Patrice Peyre, Cyril Gorny, Muriel Carin, Simon Morville, Philippe Le Masson, Denis Carron, Rémy Fabbro, 2013. Influence of various process conditions on surface finishes induced by the direct metal deposition laser technique on a Ti–6Al–4V alloy, Journal of Materials Processing Technology 213, pp. 791– 800.

G.A. Ravi, X.J. Hao, N. Wain, X. Wu, M.M. Attallah, 2013, Direct laser fabrication of three dimensional components using SC420 stainless steel, Materials and Design 47, pp. 731–736.

Donghong Ding, Zengxi Pan, Dominic Cuiuri, Huijun Li, 2015. A practical path planning methodology for wire and arc additive manufacturing of thin-walled structures, Robotics and Computer-Integrated Manufacturing 34, pp. 8–19.

Abdalla R. Nassar, Jayme S. Keist, Edward W. Reutzel, Todd J. Spurgeon, 2015, Intra-layer closed-loop control of build plan during directed energy additive manufacturing of Ti–6Al–4V, Additive Manufacturing 6, pp. 39–52.

Sörn Ocyloka, Eugen Alexeev, Stefan Mann, Andreas Weisheit, Konrad Wissenbach, Ingomar Kelbassa, 2014, Correlations of melt pool geometry and process parameters during laser metal deposition by coaxial process monitoring, Physics Procedia 56, pp.228 – 238.

Suzuki, S. and Abe, K., 1985, Topological Structural Analysis of Digitized Binary Images by Border Following, CVGIP 30 1, pp 32-46